TRN AU8306654

AAEC/E562

AAEC/E562

AUSTRALIAN ATOMIC ENERGY COMMISSION

RESEARCH ESTABLISHMENT

LUCAS HEIGHTS RESEARCH LABORATORIES

CALCULATION OF POWER TRANSIENTS FOR THE SPERT II NUCLEAR REACTOR CORE WITH INCLUSION OF NUCLEATE BOILING OF THE COOLANT

by

A.W. DALTON

February 1983

ISBN 0 642 59765 0

AUSTRALIAN ATOMIC ENERGY COMMISSION
RESEARCH ESTABLISHMENT

LUCAS HEIGHTS RESEARCH LABORATORIES

CALCULATION OF POWER TRANSIENTS FOR THE SPERT II NUCLEAR REACTOR CORE WITH INCLUSION OF NUCLEATE BOILING OF THE COOLANT

by

A.W. DALTON

ABSTRACT

The published data for a series of power transients initiated in the water-cooled core of the SPERT II nuclear reactor were investigated to determine the magnitude of the reactivity feedback effects arising from heat transfer and vapour void formation during subcooled nucleate boiling. This was done using the NAIADQ computer code which describes the thermohydraulic behaviour of the water coolant in the fuelled region of the core in terms of a set of one-dimensional linear, finite difference equations.

Nucleate boiling at the fuel surface is represented as an expanding superheated layer of water in which saturated vapour is assumed to be uniformly generated at a non-equilibrium rate. The simulation of the transients, all of which were initiated at ambient temperature, necessitated

(Continued)

the calculation of heat transfer from the fuel to the water coolant in the regimes of conduction, convection and surface boiling for a wide range of coolant flow rates during rapidly changing reactor power levels.

The calculated variations in the reactor power with time during the transients are in good agreement with the measured data over the range of conditions tested in the experimental investigations.

National Library of Australia card number and ISBN 0 642 59765 0

The following descriptors have been selected from the INIS Thesaurus to describe the subject content of this report for information retrieval purposes. For further details please refer to IAEA-INIS-12 (INIS: Manual for Indexing) and IAEA-INIS-13 (INIS: Thesaurus) published in Vienna by the International Atomic Energy Agency.

FINITE DIFFERENCE METHOD; HEAT TRANSFER; N CODES; NUCLEATE BOILING; ONE-DIMENSIONAL CALCULATIONS; REACTIVITY; REACTIVITY COEFFICIENTS; REACTOR CORES; REACTOR KINETICS; SIMULATION; SPERT-2 REACTOR; TRANSIENTS; TWO-PHASE FLOW; VAPORS; VOID FRACTION

CONTENTS

1. INTRODUCTION

Assessments of nuclear reactor safety must take into account the consequences of power transients initiated by accidental additions to the core reactivity. In a water-cooled reactor fuelled with arrays of thin metal plates containing enriched uranium, nucleate boiling at the fuel-coolant interface is initiated before bulk coolant boiling for short power periods as a consequence of the low thermal conductivity of water. Because the consequences of such power transients are sensitively dependent on the magnitude of the reactivity feedback produced in the core by the energy generated, and the fact that void formation can produce large reactivity changes, the modelling of surface boiling is of prime importance in the safety assessment of these reactor cores.

The NAIADQ computer code [Dalton 1983] has been developed specifically to calculate these effects and the series of experimental power transients on the SPERT II core [Johnson et al. 1965] was chosen to investigate its capabilities. The experimental conditions varied were the initial asymptotic period over the range 74 to 460 ms, coolant pressures from atmospheric to 1.48 MPa and coolant flow rates from zero to 12 kg s^{-1}. During the tests, the reactor power and a number of fuel surface temperatures throughout the core were measured continuously.

These transients provided a comprehensive data base for testing the code because

(a) the range of experimental conditions produced markedly different heat transfer and vapour generation rates and times at which subcooled nucleate boiling commenced; and

(b) the reactivity feedback measured during these tests showed that a large and non-linear (with energy release) component was present which could reasonably be ascribed to heat transfer and the formation of steam voids in subcooled nucleate boiling.

In the calculations, the reactor core is represented as a single fuel channel operating in the mean core flux with mean channel coolant flow. The time-dependent axial flow of the coolant in this channel is described by a set of partial differential equations which are solved numerically, using a first

order finite difference method. In the non-boiling regime, heat transfer is represented as appropriate (Section 2.2) by either a transient conduction or a forced convection model. When the water adjacent to the fuel surface reaches saturation, a surface boiling model is used to calculate the heat transfer; the associated increased rate of the latter is described in terms of the rapid propagation of a superheated temperature front into the water similar to that proposed by Connolly [1977]. It is assumed that saturated vapour is generated uniformly throughout the volume of this expanding layer (Section 2.3).

Power changes are calculated from the instantaneous values of the excess core reactivity using a point reactor kinetics model [Clancy 1983]. The excess core reactivity at any instant is derived from the sum of the initial excess reactivity and the reactivity changes produced by changes in the fuel and coolant temperatures in the core region up to that instant by the energy input to the system. Because the contribution from the changes in the fuel temperature is small, the prediction of reactivity will be sensitively dependent on the correct choice of heat transfer into the water coolant. These changes are derived from the hydrodynamic calculations, using the reactivity feedback coefficients reported by Connolly [1977]. In the boiling regime, the reactivity feedback is augmented by the large increase in the rate of heat transfer and bubble formation in the superheated layer.

2. DETAILS OF THE CALCULATIONS

2.1 The Hydraulics Model

The axial flow of the coolant along the channel is described by four conservation equations [Turner and Trimble 1978]. The quantities involved are vapour mass, mixture mass, mixture momentum and mixture energy. The conservation equations are one-dimensional in the axial direction, z, of the flow path, and at each axial position the variables in these equations (P, W, etc.) relating to the coolant fluid are expressed in terms of the averages of the local mixture properties over the flow area.

(i) Vapour Mass

$$\frac{\partial(C\rho)}{\partial t} + \frac{1}{a}\frac{\partial(CW)}{\partial z} = \Gamma \quad . \tag{1}$$

(ii) Mixture Mass

$$\frac{\partial \rho}{\partial t} + \frac{1}{a}\frac{\partial W}{\partial z} = 0 \quad . \tag{2}$$

(iii) Mixture Momentum

$$\frac{1}{a}\frac{\partial W}{\partial t} + \frac{1}{a}\frac{\partial M}{\partial z} + \frac{\partial P}{\partial z} + F + \rho \underline{g} \sin\theta = 0 \quad . \tag{3}$$

(iv) Mixture Energy

$$a\frac{\partial}{\partial t}\left(\rho H - P + \frac{M}{2a}\right) + \frac{\partial E}{\partial z} - pq + W\underline{g} \sin\theta = 0 \quad . \tag{4}$$

To obtain a solution to these equations, expressions are required for the heat flux, q, from the fuel to the coolant, the vapour generation rate Γ and the frictional pressure gradient F. Details of the latter derived for losses from the wall friction and fittings are given in Trimble and Turner [1976]. The equations used for q and Γ are described in detail below.

2.2 Heat Transfer

To calculate the power distribution between the fuel and the coolant, a one-dimensional fuel model is used in which the surface heat flux q is related to the power Q generated in the fuel by

$$q = Q - A\, dT_F/dt \quad , \tag{5}$$

where

$$q = h_T(T_F - T_L) \quad , \tag{6}$$

and

$$h_T = h_{FS}\, h_F/(h_{FS} + h_F) \quad . \tag{7}$$

2.2.1 Non-boiling heat transfer

For zero or low mass flow (Re <2000), heat is assumed to be transferred by thermal conduction. The transient thermal conduction model is based on slab geometry and an exponentially rising heat flux for which an analytical solution of the temperature distribution can be found, to give the heat

transfer coefficient at the fuel plate-water interface as

$$h_{FS} = \kappa B^2 S/(B S/\tanh(B S) - 1) \quad , \tag{8}$$

where

$$B = (\rho c/\kappa \tau_o)^{1/2} \quad . \tag{9}$$

For turbulent flow (Re >2000), a number of forced convective surface heat transfer correlations were used, all having the form

$$h_{FS} = K(\kappa/De)\, Re^n\, Pr^m \quad , \tag{10}$$

where the value of the constant K and the indices n and m depend on the option used [Dalton 1983].

2.2.2 Boiling heat transfer

For Re <2000, the surface heat transfer correlation of Forster and Zuber [1955] for pool boiling was used:

$$h_{NB} = 0.0015(\kappa/R)\, Re^{0.62}\, Pr^{0.33} \quad , \tag{11}$$

where Re and Pr are the Reynolds and Prandtl numbers for the 'flow system' associated with the bubble agitation in the superheated layer at the fuel coolant interface. For flow boiling (Re >2000), the interpolation formula of Bergles and Rohsenow [1964] was used. A correlation taken from Redfield [1965] was used to estimate the critical heat flux at which a departure from nucleate boiling occurred.

2.2.3 Selection of heat transfer correlation

(1) If the fuel surface temperature is less than the local saturation temperature of the water, a non-boiling correlation is automatically used in the calculations.

(2) When the fuel surface temperature calculated on the basis of the non-boiling option used in (1) exceeds the saturation temperature of the water, surface heat fluxes are calculated for both the non-boiling and boiling boundary conditions. If the heat flux for

nucleate boiling is greater, then it is used in the calculation; if it is smaller, then the non-boiling value of h_{FS} is used. The temperature at which the switch to nucleate boiling occurs is referred to as the trigger temperature for vapour generation.

2.3 Vapour Generation Model

2.3.1 Representation of superheated liquid

When the fuel temperature exceeds the saturation temperature of the water, it is assumed that a temperature front is propagated into the water, normal to its surface [Connolly 1977]. From the time t_1 at which this occurs, the layer of water behind this temperature front is assumed to absorb the total surface heat flux and its temperature $T_\chi(t)$ is assumed equal to that of the fuel surface. The distance advanced by the temperature front $\chi(t)$, measured from the fuel surface, at any later time t, is given by

$$\chi(t) = \int_{t_1}^{t} q \, dt \Big/ \int_{T_{L1}}^{T_{FS}} \rho(T) \, c(T) \, dT \quad , \tag{12}$$

where T_{L1} is the coolant temperature at time t_1. The integrals in this equation are solved explicitly and the values of $\chi(t)$ evaluated using parameters derived from the finite difference calculations.

2.3.2 Vapour generation

When the temperature of the superheated water reaches the trigger level, the bubbles which form at the surface of the fuel begin to grow, become detached, then rapidly increase in size. The rate at which vapour is generated is assumed to be given by the formula [Rivard and Torrey 1975]:

$$\Gamma_\chi = \lambda \, \alpha_\chi^{2/3} (1 - \alpha_\chi) (T_S Ru)^{1/2} \, (T_\chi - T_S)/T_S \quad . \tag{13}$$

To produce vapour generation when the trigger temperature is exceeded, an α 'seeding' value of 1×10^{-4} is used in the calculations.

2.4 Reactor Kinetics

The time-dependent behaviour of the reactor power is determined by using the KINET subroutine [Clancy 1983] available within the NAIADQ code to solve the reactor kinetic equations:

$$\frac{d\phi(t)}{dt} = [k(t)(1 - \beta) - 1] \frac{\phi(t)}{\ell} + \Sigma \lambda_i C_i(t) \quad , \tag{14}$$

$$\frac{dC_i}{dt} = k(t)\beta_i \frac{\phi(t)}{\ell} - \lambda_i C_i \quad . \tag{15}$$

The delayed-neutron data used in these equations [Harries 1978], which include a condensed representation of the D_2O photoneutron data of Bernstein et al. [1947], are also available within NAIADQ.

The neutron multiplication factor k(t) is found from the temperature and void distribution in the channel by means of the heat transfer and void growth equations and the temperature and void coefficients of reactivity represented by

$$k(t) = k_o + \Sigma_o^t \Delta k(t) \quad .$$

The values of $\Delta k(t)$ are calculated at each nodal point along the flow path in each successive time step cycle. The nodal contributions are axially weighted and summed to yield the total value of Δk from zero up to time t. In the non-boiling regime, the effects include fuel plate expansion, moderator expansion and neutron temperature changes in the core region:

$$\Delta k(t) = B_1 \Delta T_F + B_2 \Delta T_L + B_3 \Delta \rho_L / \rho_o \tag{16}$$

To calculate Δk arising from changes in the properties of the coolant in the boiling regime, explicit representations for the mean coolant temperature $\overline{T}_L(t)$ and density $\overline{\rho}_L(t)$ at each nodal point are used; for example:

$$\overline{\rho}_L(t) = \alpha'(t)\rho_v + (1 - \alpha'(t)) \left[\frac{\chi(t)}{S} \rho_\chi(t) + \left(1 - \frac{\chi(t)}{S}\right) \rho_L(t_1) \right] \quad , \tag{17}$$

where $\alpha'(t)$, the void ratio for the whole core, is related to that calculated for the single channel calculation $\alpha(t)$ by a 'weighting' factor ω, which takes account of the radial variation of the power distribution across the core. Reactivity changes for the coolant at any subsequent time are given by

$$\Delta k = B_3[\overline{\rho_L}(t) - \rho_0]/\rho_0 + B_2[\overline{T_L}(t) - T_L(0)] \quad . \tag{18}$$

For the temperature effects this reduces to

$$\Delta k = B_2\left[\frac{\chi}{S}\Delta T_\chi + \left(1 - \frac{\chi}{S}\right)\Delta T_L\right] \quad , \tag{19}$$

and the density effect is given to a first order approximation by

$$\Delta k = B_3\left[\omega_\alpha + \frac{\chi}{S}\frac{\Delta\rho_\chi}{\rho_0} + \left(1 - \frac{\chi}{S}\right)\frac{\Delta\rho_L}{\rho_0}\right] \quad . \tag{20}$$

2.5 Time Step Control

The magnitudes of the time steps used in the NAIADQ calculations are selected on the basis of the maximum changes in either P or H over all nodes that the user considers to be acceptable. Using this criterion, very small time steps are used only when P and H are changing rapidly.

3. COMPARISON WITH EXPERIMENT

3.1 Details of the Experiments

The SPERT II fuel plate consisted of a fuel alloy section, 62 mm x 0.51 mm x 610 mm, enclosed by cladding, 69 mm x 0.51 mm x 640 mm. Fuel plates were assembled in parallel arrays, 2.4 mm apart, in square sectioned fuel boxes with 760 mm sides, one of which is shown in Figure 1. There were 18 fuel plates to each box and 68 fuel boxes in the core; this is denoted in SPERT notation as B18/68. The core structure was immersed in heavy water contained in a 3 m o.d. reactor vessel.

The close packing of the fuel in this core caused it to be so undermoderated that the maximum thermal flux occurred in the reflector close to the boundary of the core, and the ratio of the maximum to mean core thermal flux was 2.5:1. This is illustrated in Figure 2.

Transients were initiated by rapidly ejecting a centrally located control rod from the core to bring the reactor into the required super-critical state. In all of the transients, the initial reactor power was low enough for the control rod movement to be completed before a significant amount of energy was released in the core. The low heat capacity and the high thermal conductivity

of the thin, metal fuel plates ensured that the changes in the fuel surface temperatures were in phase with the large power changes produced. The range of initiating conditions used in the tests ensured that the coolant was subjected to transient heat transfer conditions covering both the non-boiling and the boiling regimes. During the transients, the power and a number of fuel surface temperatures throughout the core were measured continuously. The excess core reactivity, obtained by inverse neutron kinetics from the power records, provided a sensitive indication of the rapid physical changes which occurred in the water coolant.

3.2 Results of the Simulation

The core of 68 fuel channels was represented axially by a single flow path operating in the mean flux with mean coolant flow rate. The geometrical properties of the materials needed for the calculations were taken from Johnson et al. [1965] and the physical properties were from Houghtaling et al. [1964]. It was assumed that the pressure drop across the core was constant throughout all the transients.

In the present report, the numbering system of Johnson et al. [1965] is used to identify the transients. The test conditions are specified in Table 1 and a comparison of the calculated and measured values of some parameters at peak power is given. The observed changes in the magnitudes of these parameters reflect the increasing contributions arising from surface boiling heat transfer effects, which are more efficient than non-boiling mechanisms in terms of reactivity feedback per unit energy released in the fuel. This is most clearly illustrated by comparing the fuel surface temperatures recorded in the highest rated channels of the experimental core with those predicted by the mean channel calculations.

The temperatures recorded in the experiments corresponded to fuel plates located at the core boundary close to the axial midplane, where the relative thermal flux level was 1.85 times the mean, as is illustrated in Figure 2. The calculated values corresponded to the axial centre of the single channel in the mean core thermal flux. For transients 8, 14, 15, 16 and 39, neither the calculated nor the measured fuel surface temperatures corresponding to these positions reached the saturation temperature of the water coolant, hence only non-boiling reactivity feedback mechanisms were involved in both the experimental and the simulated transients. The ratios of the measured to calculated fuel surface temperature rises were within the range 1.73 to 1.9

(Table 1), in very close agreement with the thermal flux ratios at the associated locations.

In the experimental transients 9, 17 and 26, boiling occurred in the maximum flux rated channels. From the time that this commenced, the temperatures in these channels rose more slowly than in the nonboiling channels, resulting in a temperature rise distribution which was no longer related to the power distribution. The extent of this deviation depended on the number of channels involved. In the simulation of these transients, the conditions for surface boiling in the mean channel were not attained, hence the ratio of experimental to calculated maximum temperature rises must be less than those predicted on the basis of the flux ratios; actual ratios ranged from 1.32 to 1.46. For the remaining nine transients, the trigger temperature for nucleate boiling was exceeded in both experiment and calculation. Hence, to some extent, the retardation in the fuel temperature rises occurred in both; ratios for this group of transients ranged from 1.01 to 1.16.

For all of the transients in which the trigger temperature was exceeded, the predicted maximum vapour void fractions varied over many orders of magnitude, as is illustrated in Table 2. This wide variation is reflected in the contribution to the reactivity compensation calculated from these vapour voids. For the no-flow tests at atmospheric pressure (runs 10-13), the voidage formation accounts for the major part of the total measured reactivity feedback. This is illustrated in Figure 3, where the calculated power and reactivity changes, both with and without vapourisation, are compared with the measured data for run 12. It is of interest to note that the void effect becomes dominant only after the time of peak power.

The calculated vapour generation rates and void ratios at axial nodes 3 to 9 are shown in Figures 4 and 5 for run 12. The whole core vapour generation rates in the supercritical transients (runs 10-13) correspond to a range of values from 90 to 250 litres per second, the same order of magnitude as the rates fitted by Connolly [1977] to the SPERT I transients.

For the remainder of the transients listed in Table 2, the calculated voidage accounted for only a very small fraction of the total reactivity compensation (Table 2), vapour generation being suppressed in these tests by the higher pressures and turbulent flow. The difference between the total reactivity compensation and that arising from vapour voids in these transients is accounted for by the non-boiling reactivity feedback effects, thermal

expansion of the water and the fuel, and changes in the neutron temperature in the core region of the reactor.

The main effect of forced coolant flow rate on the reactor power behaviour (runs 23, 25, 26 and 39) is seen after the first power peak in Figure 6 (where 'lines' correspond to the calculated data and 'points' to the measured data). Both the post-power level and the damping of the power oscillations are observed to be greater, the larger the initial rate of coolant flow. The calculations reproduced these features quite well.

The calculations also produced a detailed description of the time-dependence of the coolant flow rates induced in all the transients. With zero initial flow and large vapour generation rates, the flow behaviour is quite complicated (Figure 7; run 12). A significant flow out of both ends of the channel is produced initially by the generation of vapour within it. The subsequent rapid condensation of the vapour produces a flow reversal at the inlet end and an ultimate convective flow up the channel. The dependence of the induced flow rate on the changing void ratios at different axial positions along the channel can be seen by comparing Figures 5 and 6. For the forced flow tests, similar but much smaller effects were produced in flow behaviour, the changes being superimposed on the initial flow rate as illustrated in Figure 8 (run 23).

The calculated mean channel heat fluxes (Table 3) indicated that the critical heat flux (Section 2.2.3) is exceeded only in the maximum rated channels of the most rapid transient (run 13). Fuel burnout was observed in the peripheral channels in the corresponding experimental test.

3.3 Discussion

The uncertainty in the reactor power calibration of the SPERT cores has been quoted as ± 10 to 15 per cent [Obenchain 1969], and the estimated accuracy of the calculated reactivity feedback coefficients is better than ± 20 per cent [Connolly 1977].

Earlier studies of the SPERT II transients were made by Turner [1968] and Connolly and Harrington [1977]. The former, using a one-point model applicable only to zero flow transients, empirically fitted a boiling heat transfer and vapour generation correlation to the experimental data. Reasonably good agreement was obtained with the experimental power bursts in

which boiling occurred. Connolly and Harrington used a simple empirical model based on one-dimensional transient conduction normal to the fuel plate surface to simulate boiling heat transfer, in which the shutdown effects were assumed to arise solely from the reactivity feedback associated with increases in the density of an expanding superheated layer of coolant at the fuel-coolant interface; the contribution from the generation of vapour voids in the coolant was assumed insignificant. The good agreement with experiment over the duration of their simulations, i.e. up to the time of peak power in the no-flow transients and for several seconds beyond this point for the forced flow transients, gave support to their assumptions and indicated the need for a more detailed investigation in the hope that a sound physical base might be established for the understanding of this important facet of water-cooled reactor safety.

The model of the present investigation, which contains a detailed description of the thermohydraulics of the coolant along the axial direction of the flow path, and of nucleate boiling in which vapour generation is included, attempts to provide such a basis. With this model, agreement as good as that obtained by Connolly and Harrington [1977] was obtained over the time period common to both simulations for all transients. The significance of this agreement lies in the fact that, in the present simulations, the calculated reactivity feedback arising from vapour generation was insignificant, hence providing support for the assumptions made in both models for these transients. However, beyond the time of the power peak for the zero flow transients, the NAIADQ model predicted that the major contribution to the reactivity feedback arises from vapour generation in surface nucleate boiling. That such good agreement was also obtained for these transients (discussed below) provided further support for the validity of the models used in the code.

The vapour void fractions present at any instant during these transients depend not only on the level of superheat in the expanding two-phase layer but also on the thickness of the layer at that instant (determined by the sub-cooling of the bulk coolant in the channel) and the time at which the trigger temperature for vapour generation is exceeded [Hahne and Grigull 1977]. For the zero flow tests at atmospheric pressure, the observed differences in vapour generation rates (Table 2) reflect the differences in the superheat reached by the layer. The large differences observed between the zero flow tests at atmospheric and at high pressure reflect the large differences in the sub-cooling of the bulk coolant in the respective tests. The large

differences in the vapour generation (Table 3), between runs 18 and run 10 for example where the superheats differ by only 4.5 K, arise from the 120 K difference in the sub-cooling of the bulk coolant between the two transients.

The low vapour void fractions found in the flow tests were also a consequence of the large sub-cooling of the bulk coolant, the small systematic variation within the flow tests arising from increase in the trigger temperature and the decrease in maximum fuel surface temperature with flow rate (Table 3). Thus in run 26, although the maximum temperature exceeded the coolant saturation temperature, no vapour was generated because the trigger temperature was not attained. For run 39 the maximum temperature was 70 K below the saturation temperature of the coolant.

The agreement obtained for the flow transients, in which the observed effects were primarily a consequence of the rate of energy removal from the core region by the forced coolant flow and the heat transfer in nucleate boiling, therefore provides good support for both the thermohydraulics calculation and the use of the steady state heat transfer correlations for turbulent flow during rapid transient conditions. The agreement obtained for the no-flow transients, in which large peak values of reactivity compensation were observed, supports the use of the non-equilibrium vapour generation model for transients in which rapid changes in heat transfer rates occur during subcooled nucleate boiling.

A more complete comparison could have been made if the coolant temperatures, pressures and mass flow rates in the core had been included in the published data, the data calculated by the code being much more extensive. In particular, the heat transfer correlations and the vapour generation model used in the present analysis could have been checked more directly. A confirmation of the induced effects observed in the calculated flow rates of the coolant in all the transients would have provided good support for the thermohydraulics calculations.

4. CONCLUSIONS

The model used in the present analysis was in good agreement with the published experimental data for both the boiling and the non-boiling transients over a wide range of flow conditions, including zero flow. It indicated that, even for power transients in which the fuel surface

temperature rose rapidly through the saturation temperature, the ensuing reactivity compensation produced by nucleate boiling at the fuel surface was sufficient to ensure that such transients can be self-limiting before the formation of large vapour voids in the bulk coolant flow. For the zero flow transients, in which large vapour voids were produced, the calculations showed that their occurrence coincided with the return of the reactor power to a very low level following the rapid rise to peak value, and hence were not instrumental in the termination of the excursion.

That this agreement with the measured data was obtained using a vapour generation and hydraulics model similar to that successfully applied in depressurisation codes used to simulate loss of coolant accidents [Dalton 1983; Rivard and Torrey 1975] adds to the generality and validity of this method of analysis. On the basis of the agreement obtained in these simulations, the NAIADQ code appears to be a promising method for investigating thermodynamic non-equilibrium in two-phase flow.

5. ACKNOWLEDGEMENTS

The author wishes to thank W.J. Turner and J.W. Connolly for their assistance in the development of the code, G.D. Trimble and W.J. Turner for the provision of the hydraulics code on which the present code is based, and B.E. Clancy for his assistance with the utilisation of the point reactor kinetics code.

6. REFERENCES

Bernstein, S., Preston, W.M., Wolfe, G. and Slattery, R.E. [1947] - Yield of Photo-neutrons from ^{235}U Fission Products in Heavy Water. Phys. Rev., 11:573-582.

Bergles, A.E. and Rohsenow, W.M. [1964] - The Determination of Forced-convection Surface Boiling Heat Transfer. J. Heat Transfer, 86:365.

Clancy, B.E. [1983] - ZAPP - A Computer Program for the Simulation of Power Reactor Transients. AAEC/E report (to be published).

Clancy, B.E., Connolly, J.W. and Harrington, B.V. [1975] - An Analysis of Power Transients Observed in SPERT I Reactors. AAEC/E345.

Connolly, J.W. [1977] - A Simple Method of Transient Heat Transfer and its Application to Power Excursions in Water Moderated Nuclear Reactors. Second Australasian Conference on Heat and Mass Transfer. University of Sydney, February, pp. 485-492.

Connolly, J.W. and Harrington, B.V. [1977] - An Analysis of Power Transients Observed in the SPERT II D_2O Moderated Close Packed Core. AAEC/E418.

Dalton, A.W. [1983] - NAIADQ - A Computer Code for Calculating Power Transients in Experimental Nuclear Reactors. AAEC/E report (in preparation).

Forster, H.K. and Zuber, N. [1955] - Dynamics of Vapour Bubbles and Boiling Heat Transfer. AIChE J., 1:531-535.

Hahne, E. and Grigull, U. [1977] - Heat Transfer in Boiling. Academic Press, New York, London.

Harries, J.R. [1978] - Inverse Kinetics Reactivity Measurements on the Materials Testing Reactor, HIFAR. AAEC/E456.

Houghtaling, J.E., Sala, A. and Spano, A.H. [1964] - Transient Temperature Distributions in the SPERT I D12/25 Fuel Plates During Short-period Power Excursions. IDO-16884.

Johnson, R.L., Lawson, H.A., McClure, J.A. and Norberg, J.A. [1965] - An Analysis of the Excursion Behaviour of a Highly Enriched Plate - Type D_2O - Moderated Core in SPERT II. IDO-17109.

Obenchain, C.F. [1969] - PARET - A Programme for the Analysis of Reactor Transients. IDO-17282.

Redfield, J.A. [1965] - CHIC-KIN - A Fortran Program for Intermediate and Fast Transients in a Water Moderated Reactor. WAPD-TM-479.

Rivard, W.C. and Torrey, M.D. [1975] - Numerical Calculations of Flashing from Long Pipes Using a Two-field Model. LA-6104-MS.

Shrock, V.E. [1966] - Reactor Heat Transients Research - Final Report - Transient Boiling Phenomena. SAN-1013.

Trimble, G.D. and Turner, W.J. [1976] - NAIAD - A Computer Program for Calculation of the Steady State and Transient Behaviour (Including LOCA) of Compressible Two-phase Coolant in Networks. AAEC/E378.

Turner, W.J. [1968] - Calculation of 'SPERT' Transients. J. Nucl. Energ., 22:397-409.

Turner, W.J. and Trimble, G.D. [1978] - AAEC private communication.

Vapour generation rate in coolant	Γ
Relaxation constants of delayed neutrons	λ_i
Constant in vapour generation formula	λ
Neutron density	ϕ
Density of coolant	ρ
Angle of elevation	θ
Asymptotic period of power transient	τ_o
Spatial weighting for void reactivity	ω
Thickness of superheated water layer	χ

Subscripts

F	Fuel mean	tm	Time of peak power
FS	Fuel surface	tr	Trigger
L	Bulk liquid	T	Total
max	Maximum	V	Vapour
NB	Nucleate boiling	χ	Superheated region
S	Saturation	o	Time zero

7. NOTATION

SI units are used for all variables.

Heat capacity per unit heated wetted area	A
Flow area of flow path	a
Core reactivity feedback coefficients	
fuel expansion	B_1
neutron temperature	B_2
coolant expansion	B_3
Specific heat of coolant	c
Precursor concentrations	C_i
Quality of coolant (non-equilibrium)	C
Equivalent diameter of coolant channel	De
Energy flux of mixture	E
Frictional pressure gradient	F
Acceleration due to gravity	g
Heat transfer coefficient	h
Enthalpy	H
Multiplication factor for core flux	k
Prompt neutron lifetime	ℓ
Momentum of coolant x flow area	M
Pressure of coolant	P
Heated perimeter of fuel	p
Prandtl number	Pr
Heat flux at fuel surface	q
Power generated per unit heated area	Q
Mean bubble radius	R
Universal gas constant	Ru
Reynolds number	Re
Half fuel plate separation	S
Temperature	T
Real time	t
Mass flow rate of coolant	W
Axial distance along flow path	z
Void fraction in coolant	α
Delayed neutron fraction	β
Fission energy release	ξ
Thermal conductivity of coolant	κ

TABLE 1

COMPARISON OF EXPERIMENTAL AND CALCULATED DATA

Run No.	Pressure (MPa)	Mass Flow (kg s^{-1})	Inverse Period (s^{-1})	Initial Temp. (K)	ϕ_{max} Core Power (MW)			$\xi_{tm}/\tau_0\ \phi_{max}$			$(T_x - T_o)_{tm}$ (K)		
					Expt	Calc.	Ratio	Expt	Calc.	Ratio	Expt	Calc.	Ratio
8	0.110	0	2.17	295	16	17	0.95	2.32	2.13	1.09	95	50	1.9
9	0.110	0	4.40	295	42	39	1.08	2.09	2.40	0.87	105	71	1.48
10	0.110	0	6.30	295	106	108	0.98	1.51	1.62	0.93	122	105	1.16
11	0.110	0	9.07	295	189	195	0.97	1.39	1.41	0.99	133	114	1.16
12	0.110	0	11.4	295	237	270	0.88	1.45	1.39	1.04	139	120	1.16
13	0.110	0	13.5	295	287	351	0.82	1.47	1.35	1.08	147	125	1.18
14	2.58	0	3.5	293	38	37	1.03	2.01	2.00	1.01	131	72	1.82
15	2.58	0	5.5	295	79	88	0.89	2.08	1.96	1.06	208	116	1.79
16	2.58	0	4.0	295	47	48	0.98	2.01	2.00	1.00	144	83	1.73
17	2.58	0	6.4	294	97	126	0.77	1.96	1.91	1.03	212	145	1.46
18	2.58	0	10.3	295	241	318	0.76	1.71	1.73	1.01	256	227	1.13
20	1.48	0	10.0	295	-	298	-	-	1.67	-	200	198	1.01
21	1.48	0.37	11.0	295	266	261	1.02	1.64	1.60	1.03	190	188	1.05
23	1.48	1.2	11.0	295	265	268	0.99	1.72	1.61	1.07	198	193	1.03
25	1.48	3.0	11.0	297	257	273	0.94	1.81	1.61	1.12	186	178	1.04
26	1.48	6.0	10.0	300	263	273	0.96	1.15	1.64	1.06	193	146	1.32
39	1.48	12.0	9.5	313	248	239	1.04	2.09	2.06	1.01	180	101	1.78

TABLE 2

MAXIMUM VALUES OF VAPOUR GENERATION PROPERTIES DURING THE TRANSIENTS

Run No.	Generation Rate ($kg\ m^{-3}\ s^{-1}$)	Void Fraction	Reactivity Compensation ($)			
			Voidage	Total		
			Calc.	Calc.	Expt.	Ratio
10	1.5	0.34	2.57	3.15	3.65	0.86
11	2.4	0.52	3.93	5.42	5.05	1.07
12	3.3	0.65	4.91	5.81	6.30	0.92
13	4.2	0.71	5.37	6.64	6.94	0.95
18	0.036	0.0004	0.003	2.42	2.02	0.83
20	0.100	0.0024	0.018	2.36	-	-
21	0.094	0.0022	0.017	2.42	2.18	0.89
23	0.079	0.0019	0.014	2.41	2.21	0.91
25	0.068	0.0017	0.013	2.40	2.04	0.85

TABLE 3

CALCULATED FUEL SURFACE TEMPERATURES AND HEAT FLUXES

Run No.	T_S (K)	T_{tr} (K)	T_{max} (K)	$T_{max} - T_{tr}$ (K)	$T_{max} - T_S$ (K)	Heat Flux ($MW\ m^{-2}$)	
						Max.	Critical
8	375.5	-	367.2	-	-	0.07	4.6
9	"	-	387.3	-	-	0.21	3.8
10	"	394.0	403.0	9.0	27.5	1.0	3.3
11	"	"	411.3	17.3	35.8	1.6	3.7
12	"	"	416.7	22.7	40.1	2.1	4.2
13	"	"	421.5	27.5	45.9	2.7	4.8
14	499.2	-	377.5	-	-	0.21	13.1
15	"	-	448.3	-	-	0.45	9.8
16	"	-	404.6	-	-	0.26	12.2
17	"	-	484.2	-	-	0.63	7.7
18	"	513.5	522.3	8.8	23.1	2.7	11.1
20	470.8	486.0	496.5	10.5	25.7	2.5	7.1
21	"	484.4	495.0	10.4	24.2	2.1	7.3
23	"	486.3	494.5	8.2	23.7	2.2	8.2
25	"	488.6	494.0	5.4	23.2	2.1	10.8
26	"	-	473.0	-	2.2	1.9	13.0
39	"	-	424.9	-	-	1.9	16.0

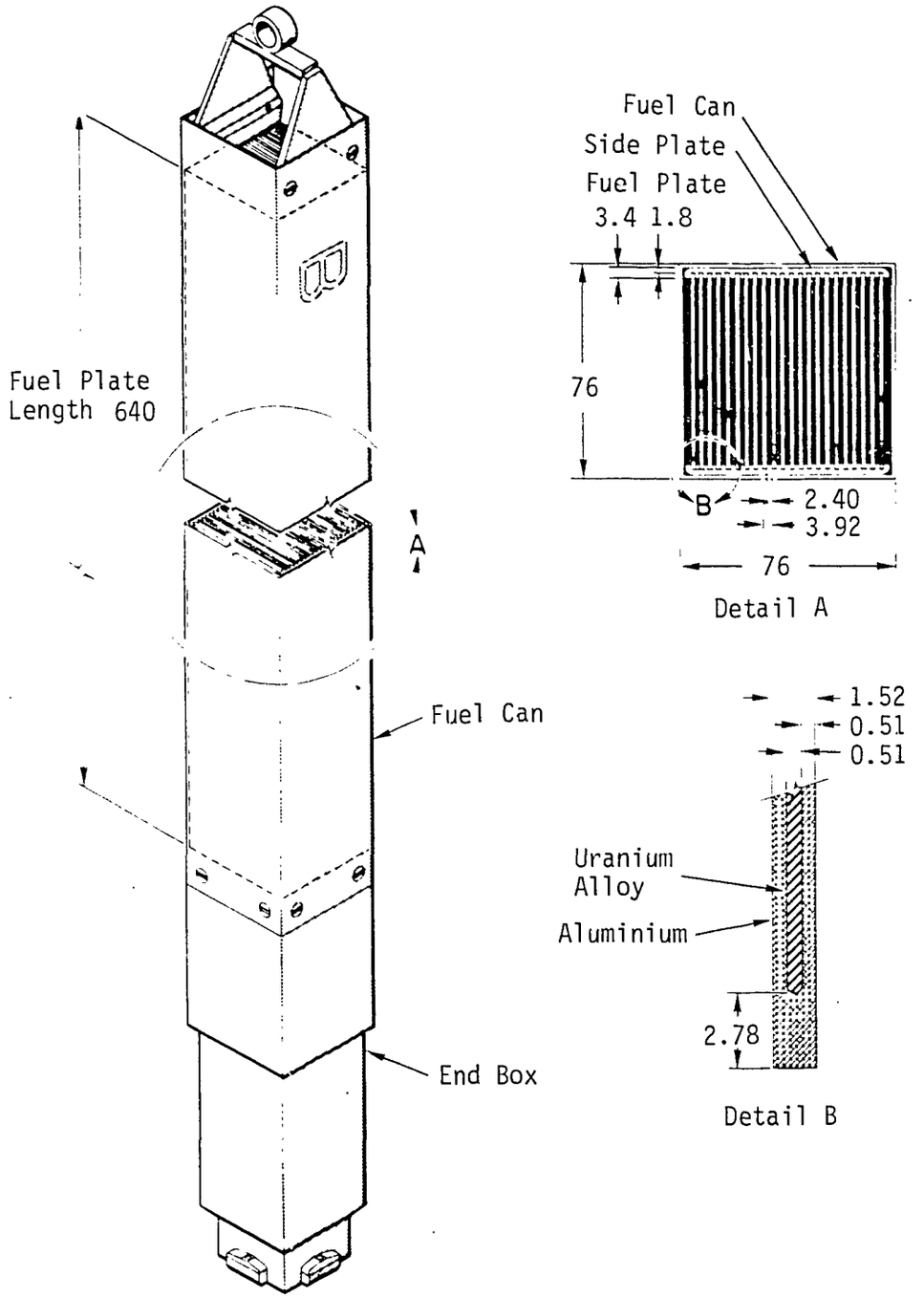

NOTE: All dimensions are given in mm

FIGURE 1. SPERT II FUEL ASSEMBLY
(After Johnson et al. 1965)

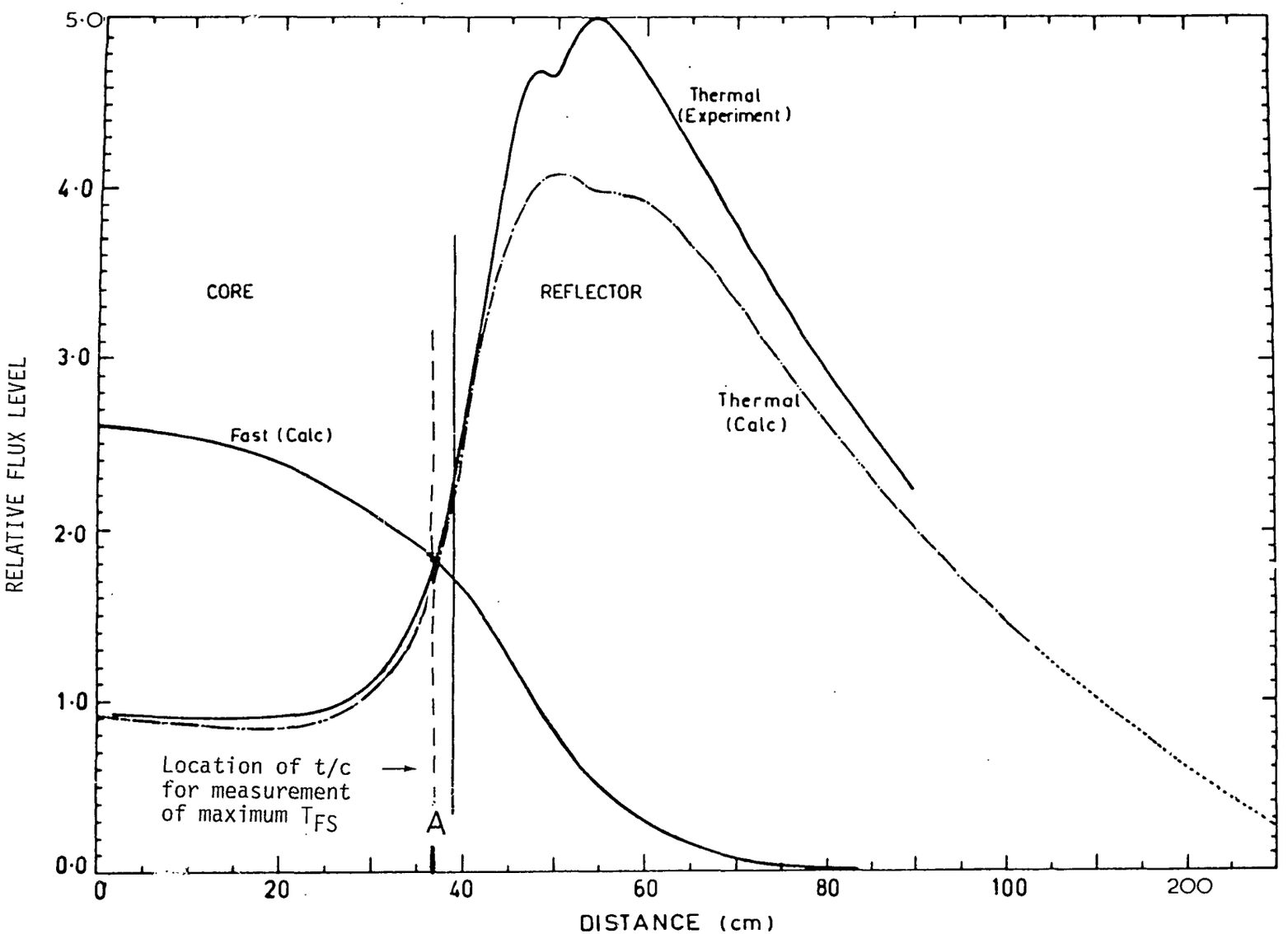

FIGURE 2. RADIAL FLUX DISTRIBUTIONS
(After Connolly 1977)

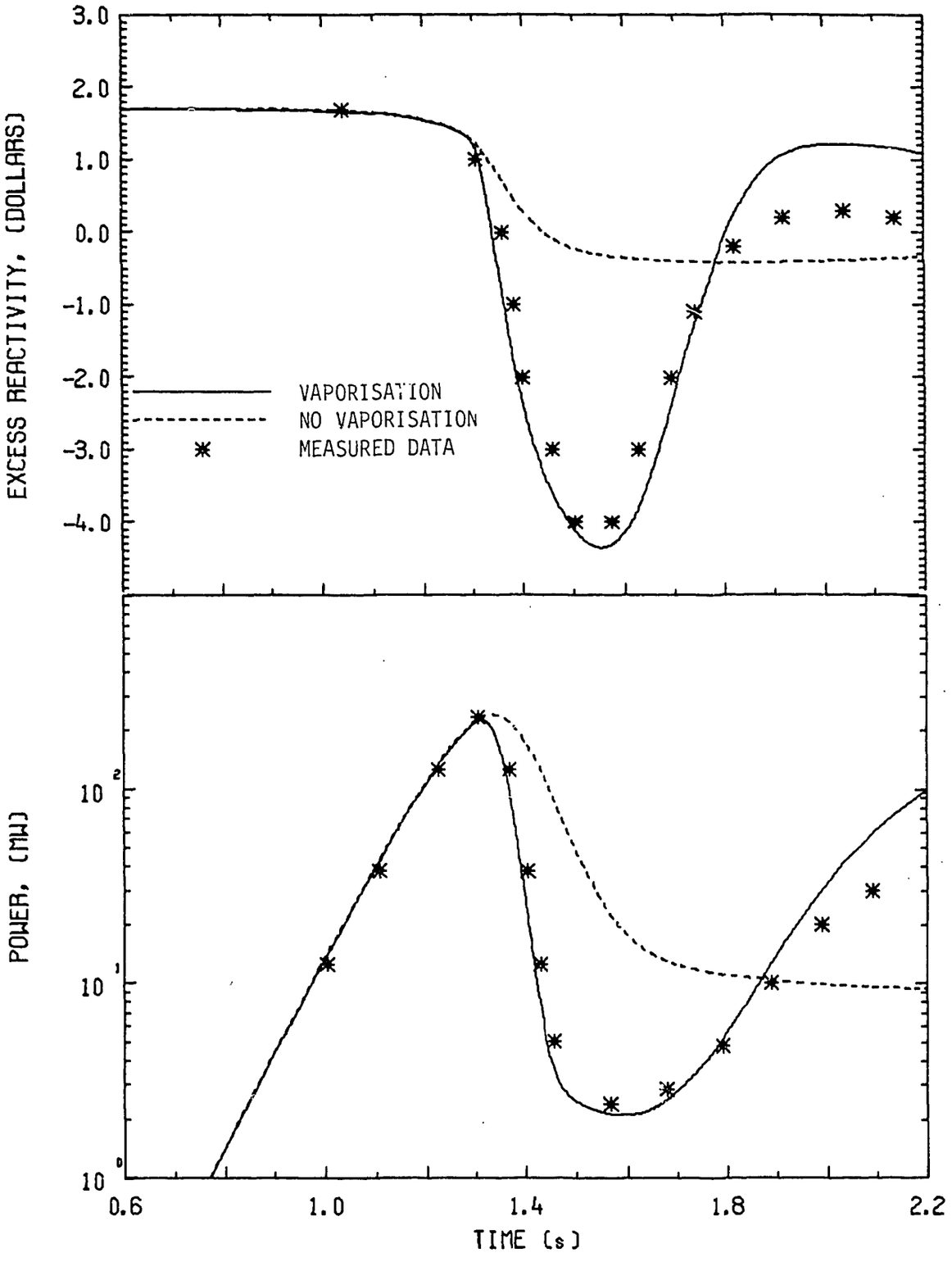

FIGURE 3. EFFECT OF VAPORISATION ON POWER AND EXCESS REACTIVITY

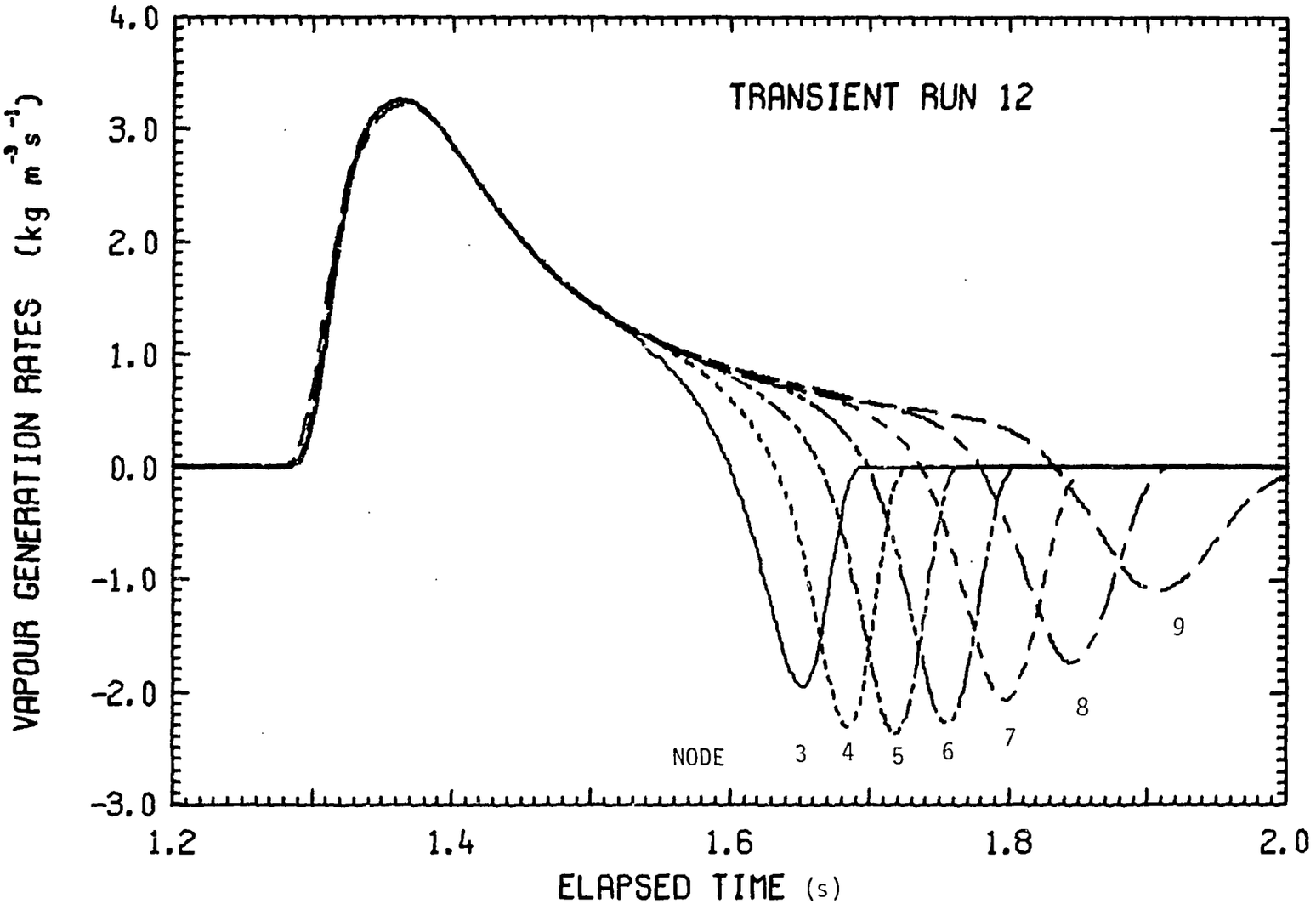

FIGURE 4. PREDICTED VAPORISATION RATES ALONG THE CHANNEL

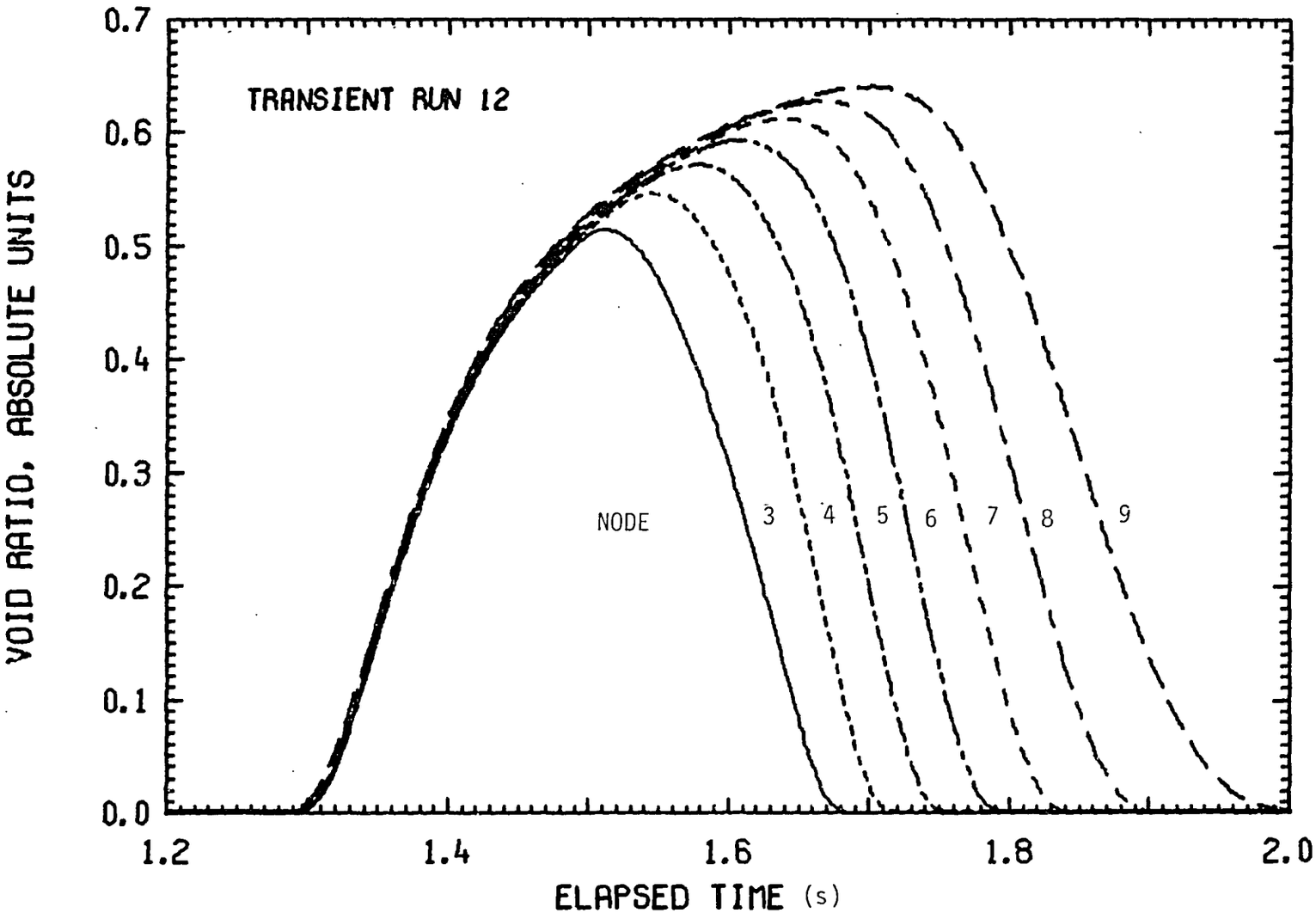

FIGURE 5. PREDICTED VOID RATIOS ALONG THE CHANNEL

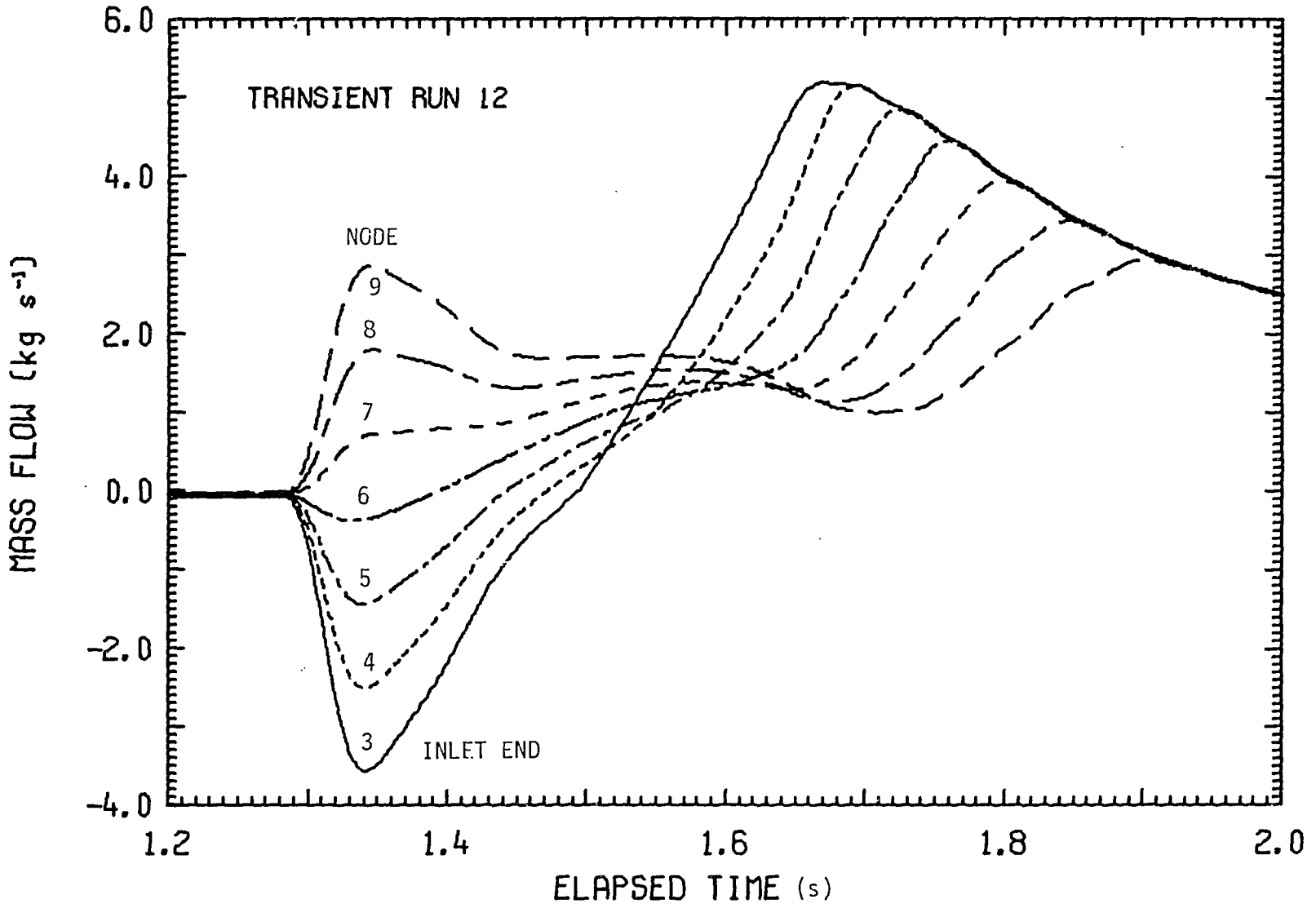

FIGURE 6. PREDICTED MASS FLOW RATES ALONG THE CHANNEL

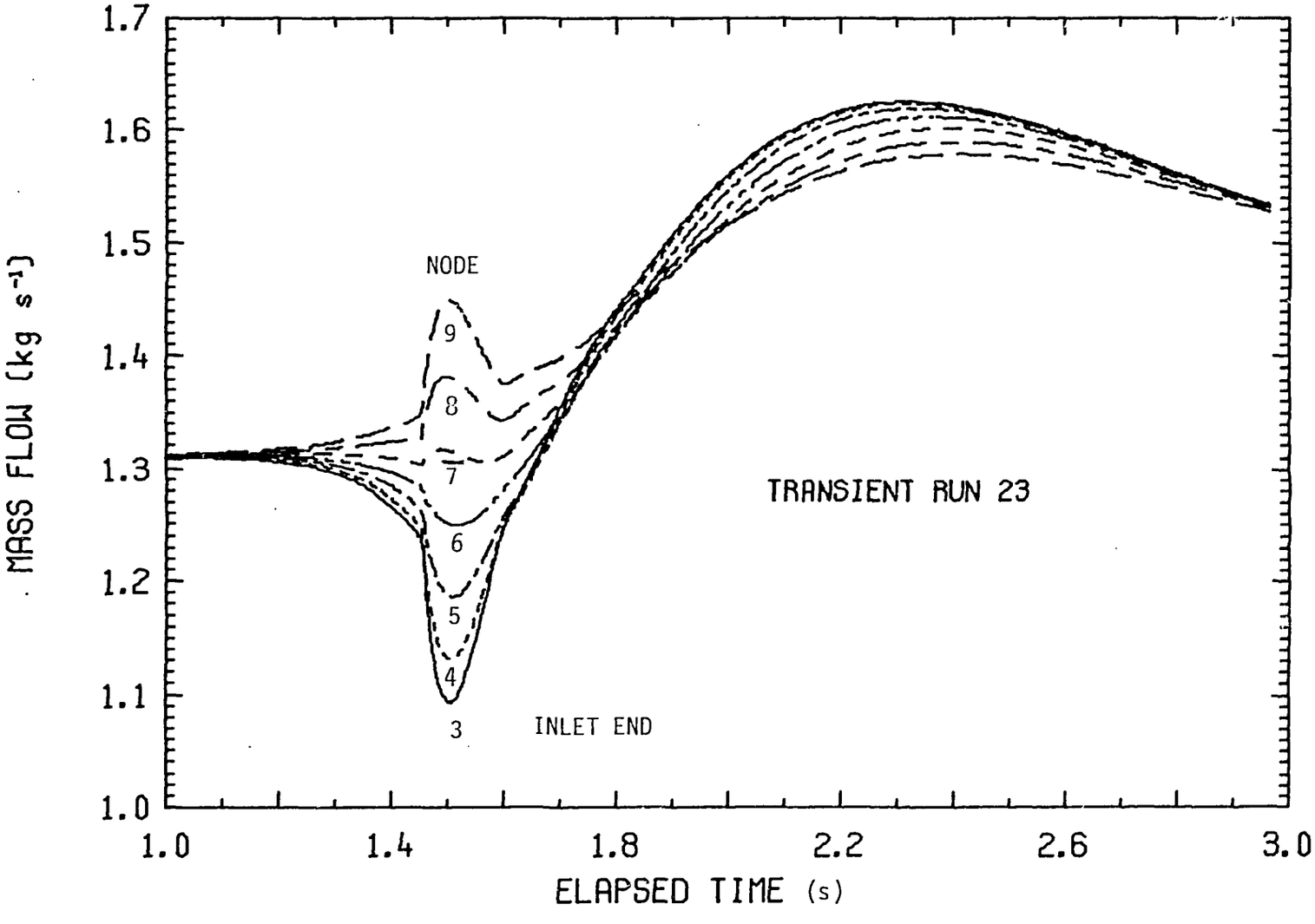

FIGURE 7. PREDICTED MASS FLOW RATES ALONG THE CHANNEL

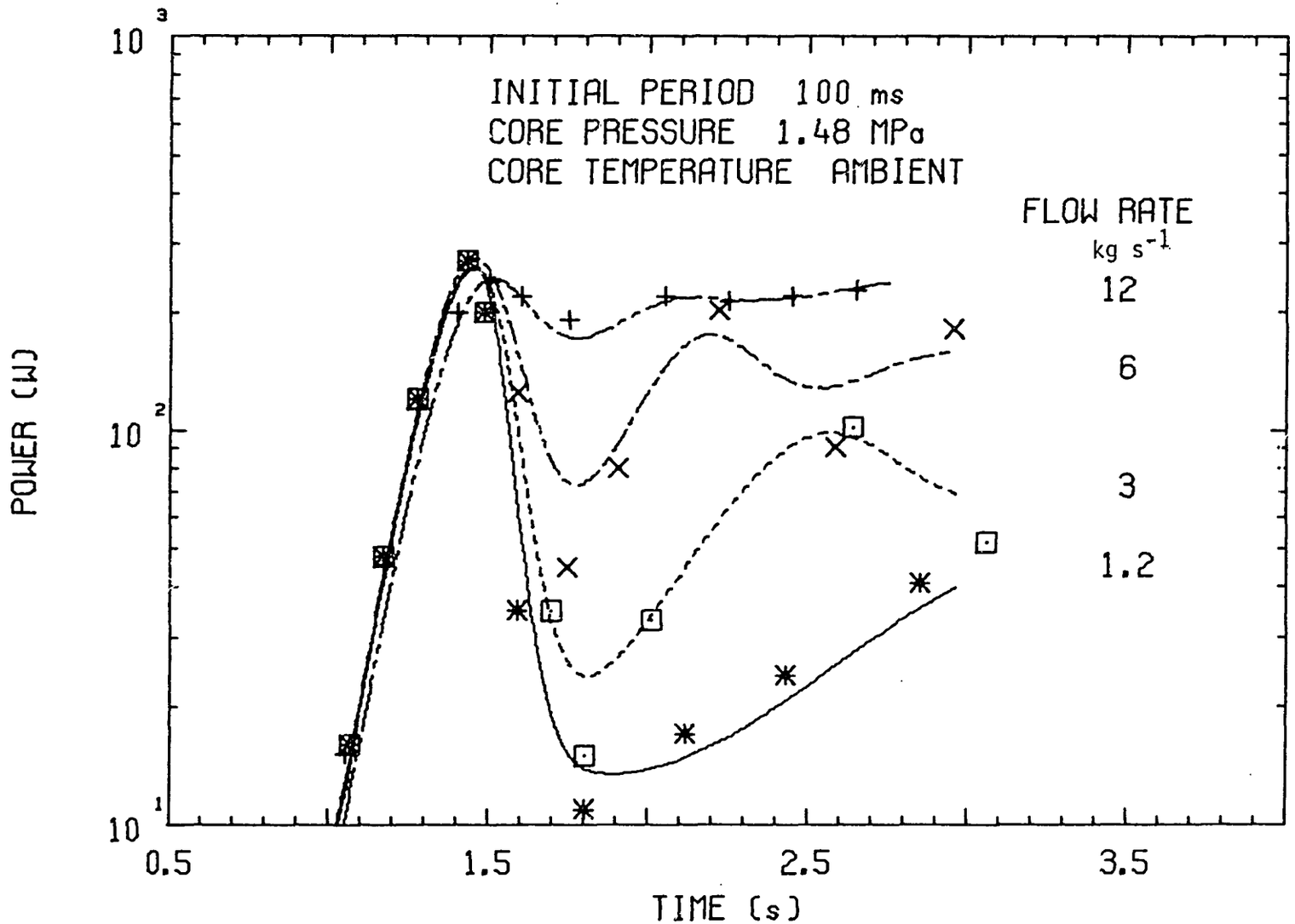

FIGURE 8. PREDICTED POWER CHANGES IN THE FLOW TESTS